WEP Warwick Evans Publishing

International Journal of Computer Science and Information Technology

ISSN: 3005-9682 (Print), ISSN: 3005-7140 (Online) | Volume 4, Number 3, Year 2024
DOI: https://doi.org/10.62051/ijcsit.v4n3.11
Journal homepage: https://wepub.org/index.php/IJCSIT/index

Improving Real-Time Gear Contact Fatigue Inspection with Machine Vision

Hai Li *, Xiaoyang Wang, Shihui Wu, Songze Ye

College of Electromechanical and Information Engineering, Chongqing College of Humanities, Science and Technology, No. 256 College Street, Caojie Town, Hechuan District, Chongqing, 401524, China

ABSTRACT

A fast gear image correction algorithm is proposed for the real-time detection of gear pitting failure area in gear contact fatigue test. Based on the fact that gear pitting first appears near the pitch circle of the gear and expands to the root circle [1], the algorithm uses the pitch circle as the basis for the camera scanning line frequency calculation, and uses the pitch circle as the segmentation point to calculate the actual pixel value of the gear meshing surface, which leads to a reduction in the amount of computational parameters. The trigonometric function calculation method instead of the involute parametric equation curve product formula is used, which makes the calculation speed increase. Based on the principle of involute gear meshing and the principle of scanning camera shooting, the pixel value of gear meshing surface imaging is deduced, as well as the formula for calculating the pitting rate of gears based on the pixel value is proposed. The experimental results show that the average absolute error of the gear image fast correction algorithm proposed in this paper is 2.2868%, and the average relative error is 0.11059mm2, the algorithm is relative to the gear mesh surface correction algorithm [2] in the detection of the gear pitting area of the absolute error decreases by 0.1412%, and the relative error decreases by 0.0127mm2, and the computational complexity for the gear mesh surface correction algorithm 1/5 of that of the gear mesh surface correction algorithm, and finally combined with the pixel value-based gear pitting rate calculation formula, thus accurately detecting the time of gear pitting failure.

KEYWORDS

AI Strategy Games; Mini-Max Algorithm; Board Game Digitisation; Spellcaster; LibGDX

1. INTRODUCTION

Contact fatigue is a surface fatigue damage phenomenon of contact materials whose contact surfaces form pits or pockmarks under the action of long-term cyclic contact stresses, and this phenomenon will make the materials in the work of increased noise, wear and tear, vibration and temperature rise, which will lead to material failure, and even cause the damage of the whole machine [1-3]. Gear contact fatigue failure is a failure mode with the highest incidence of all closed gear failure forms, and its main manifestation is pitting failure. Gear pitting failure will lead to increased transmission gear vibration noise, affecting transmission efficiency, and may even lead to transmission system paralysis, triggering dangerous accidents. The most effective way to study gear contact fatigue failure is to obtain the gear contact fatigue failure curve through gear contact fatigue test, so it is important to accurately obtain the time point of fatigue micro-pitting initiation as well as the time point of pitting failure for the study of gear contact fatigue curve [4-8].

At present, the main detection methods used in gear contact fatigue test are human eye observation method, fluorescent coating method, vibration detection method and so on. However, these methods

cannot visually record the evolution of gear contact fatigue, not to mention quantitative detection of fatigue failure [9-11]. Gear contact fatigue pitting real-time detection method based on machine vision in the paper designed gear contact fatigue detection system [2], which realizes the quantitative detection of gear fatigue pitting and on-line detection, but due to the complex design of the detection algorithm and the large number of parameters that need to be computed, which leads to the slow speed of computation, and can not achieve the accurate time of the fatigue failure judgment, so the main focus of this paper's research is to find out how to reduce the gear fatigue pitting detection algorithm computational complexity, improve the detection speed, and obtain the accurate time of gear fatigue failure.

According to the gear fatigue pitting first occurs in the vicinity of the pitch circle, and gradually expand to the root circle, therefore, this paper proposes gear image fast correction algorithm. The algorithm uses the radius of the pitch circle to calculate the camera line frequency, and divides the gear meshing surface into two parts, the top circle to the pitch circle and the pitch circle to the tooth root circle, and calculates the occupied pixel value separately, so as to avoid dividing the gear meshing surface into multiple sections of the tooth contour to calculate the pixel value occupied by each section of the tooth contour, and thus to reduce the computational complexity. On the other hand, the algorithm adopts the idea of replacing curves with straight ones, approximating involute curves as trigonometric straight line segments, thus avoiding the use of parametric equations of curves to find the product formula and improving the detection speed. Finally, the formula for calculating the pitting rate of gears corresponding to the pixel value is given, thus realizing the rapid calculation of the pitting rate of gears and the accurate detection of the fatigue failure time of gears.

2. GEAR VISION INSPECTION SYSTEM OVERALL PROGRAM DESIGN

In order to ensure that a clear and complete image of the working area of the gear is obtained when the gear is rotating at 500r/min, a line array camera is used in this paper, and the entire complete image of the working surface of the gear is obtained by placing the camera in an eccentric manner. To guarantee that the collected images are always in clear and high quality images, telecentric lenses are selected, and finally the gear visual inspection system is built.

2.1. Camera Options

The camera is the core part of the visual inspection system, the role is to convert the light signal reflected from the surface of the object into an electrical signal, the quality of the image acquisition is mainly the acquisition system sensor decision [4]. The core parameters of a line array camera include resolution, line frequency, and image original size. To obtain images of the meshing surfaces of the gears in operation, a line array camera, model data-02A04K, with a resolution of 2048 × 1 pixels and a maximum line frequency of 80 kHz, was selected.

Equation for conversion between acquisition line frequency and gear speed for a line array camera:

$$\delta = l / \beta \tag{1}$$

$$LF = \frac{L_t n}{60\delta} \tag{2}$$

Where β is the camera magnification, β= 0.2; l is the pixel size, l = 7.04 μm; δ is the actual length corresponding to a pixel size, unit μm; LF is the line frequency of the line array camera; n is the gear rotation speed, unit r/min; Lt is the length of the whole image obtained by the camera scanning when the gear rotates one week, unit mm.

2.2. Optimal Camera Position

Most of the gear contact fatigue tests use involute straight toothed cylindrical gears in order to facilitate the calculation of fatigue pitting area and failure determination. Therefore, the present study is carried out for pitting corrosion of involute straight toothed cylindrical gears with the test gear module m = 2mm, tooth number z = 28 and tooth width 20mm.

In order to obtain a clear image of the entire gear meshing surface, the eccentric shooting method is used. As shown in Figure 1, h is the optimal eccentricity distance in mm; ra and rb are the radii of the gear tooth apex circle and base circle respectively in mm.

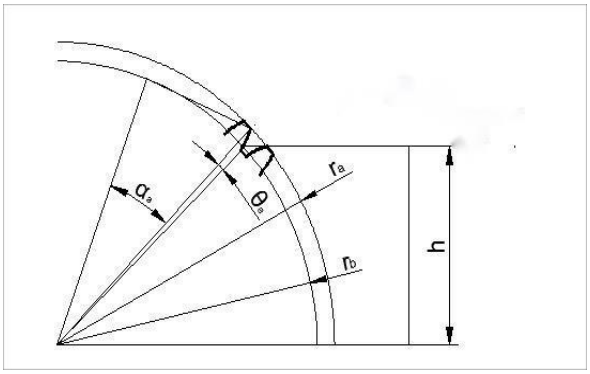

Figure 1. Optimal Shooting Height

Combined with the characteristics of the scanning camera, the image of each tooth of the gear obtained consists of two parts: one is the image of the entire meshing surface of the gear from the base circle to the top circle, and the other is the image of the tooth thickness of the top circle. In order to calculate the optimal eccentricity shooting distance h, establish a right-angle coordinate system x1O1y1 as shown in Fig. 2, in which the origin O1 is the center of the gear circle, the point C1 is the base circle and the involute intersection of a tooth on the gear and the line connecting the points O1 and C1 as the x1-axis, and the straight line perpendicular to the x1-axis and passing through the origin O1 is the y1-axis.

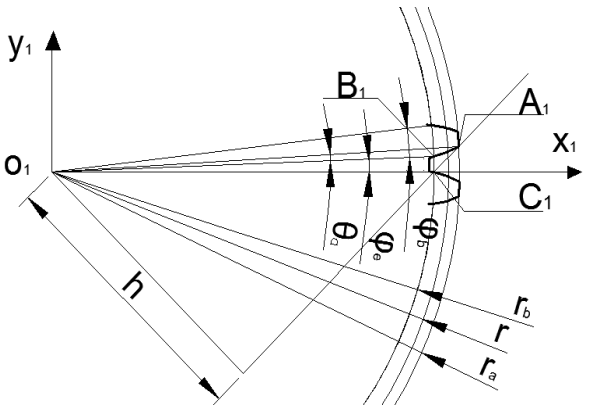

Figure 2. Resolution of the optimal eccentric shooting distance of the camera.

To calculate the optimal eccentric shooting distance h, the equation of the line A1C1 needs to be found first. And under the coordinate system x1O1y1, the coordinates of point C1 are (rb, 0) and the coordinates of point A1 (xa, ya) are:

$$x_a = r_a \cos \omega_a \tag{3}$$

$$y_a = r_a \sin \omega_a \tag{4}$$

Where ra is the radius of the tooth apex circle; ωa is the angle between O1A1 and the x1-axis, and:

$$\omega_a = \varphi_e + \theta_a \tag{5}$$

θ_a is the spreading angle in rad of the involute of the tooth apex circle; φ_e is the angle in rad corresponding to the slot width of the base circle.

It can be seen that the key to determining the optimal eccentric shooting distance is to calculate θ_a and φ_e.

(1) Calculation of θ_a

The gear involute principle is shown in Figure 3.

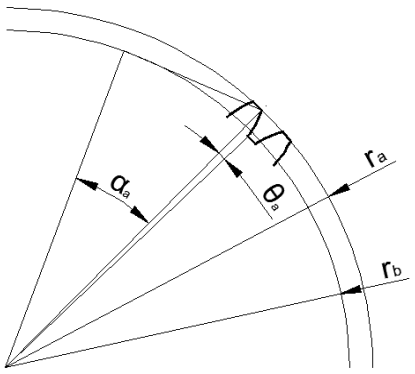

Figure 3. Gear involute principle

The equation of the involute of the tooth apex circle is:

$$\begin{aligned} \theta_a &= \text{inv}\alpha_a = \tan\alpha_a - \alpha_a \\ r_a &= r_b / \cos\alpha_a \\ r_b &= \frac{1}{2} mz\cos\alpha \end{aligned} \tag{6}$$

In the formula, α_a is the pressure angle of the involute of the tooth apex circle; α_a is the pressure angle of the indexing circle, α = 20°; the meaning of the rest of the parameters is the same as before.

And the tooth apex circle radius r_a and indexing circle radius r are respectively:

$$r_a = \frac{1}{2} mz + h_a^* m \tag{7}$$

$$r = \frac{1}{2} mz \tag{8}$$

In the formula, ha* for the top of the tooth height coefficient, ha*=0.8; the rest of the parameters have the same meaning as before.

(2) Calculation of φ_e

The gear selected for the test is a standard short system of teeth, and the installation method is standard installation. Therefore, the base circle tooth pitch Pb and base circle tooth thickness Sb are respectively:

$$P_b = \pi m\cos\alpha \tag{9}$$

$$S_b = S\cos\alpha + 2r_b\text{inv}\alpha \tag{10}$$

Where S is the thickness of the indexing circle; the rest of the parameters have the same meaning as before.

And the base circle tooth pitch is equal to the base circle tooth thickness plus the base circle slot width, so the base circle slot width Pe is:

$$P_e = P_b - S_b \tag{11}$$

The base circle groove width is divided by the base circle radius to find the angle corresponding to the base circle groove width φ_e. Substituting the calculated θ_a and φ_e into Eq. (5) yields the angle between O1A1 and the x1-axis ωa, Substituting into equations (3) and (4), we obtain the coordinates of point A1 (xa, ya), which in turn leads to the equation of the line A1C1:

$$y - \frac{y_a}{(x_a - r_b)} x + \frac{y_a r_b}{(x_a - r_b)} = 0 \tag{12}$$

Where A, B, and C are the coefficients of the linear equation A1C1, respectively; (x0, y0) are the coordinates of the point O1.

The above analysis shows that the optimum eccentric shooting distance is related to four parameters: module of the gear, number of teeth, pressure angle of the indexing circle, and top height coefficient of the teeth.

For the test gear, θ_a = 0.0395 rad, φ_e = 0.0824 rad, ωa = 0.1219 rad, the coordinates of point A1 (29.3804, 3.5990), and the coordinates of point C1 (26.3114, 0), the equation of the line A1C1 is:

$$y - 1.1727x + 30.8558 = 0 \tag{13}$$

The resulting optimal eccentric shooting distance of the camera is h = 20 mm.

2.3. Image Acquisition System Construction

In order to realize the accurate adjustment of the eccentricity distance of the camera, a precision lifting table is chosen. In order to improve the quality of image acquisition, a light source holder that can be precisely adjusted in x, y and z directions is designed. Meanwhile, in order to enhance the contrast between the pitting pits and the normal tooth surface, the gears selected for the test were blackened. A gear contact fatigue test bench is built, and then a gear contact fatigue image acquisition system is built by combining the previously selected camera, light source, telecentric lens, light source keeping stand and the derived optimal camera shooting position as shown in Fig. 4. The original image of the gear is captured with this system as shown in Fig. 5.

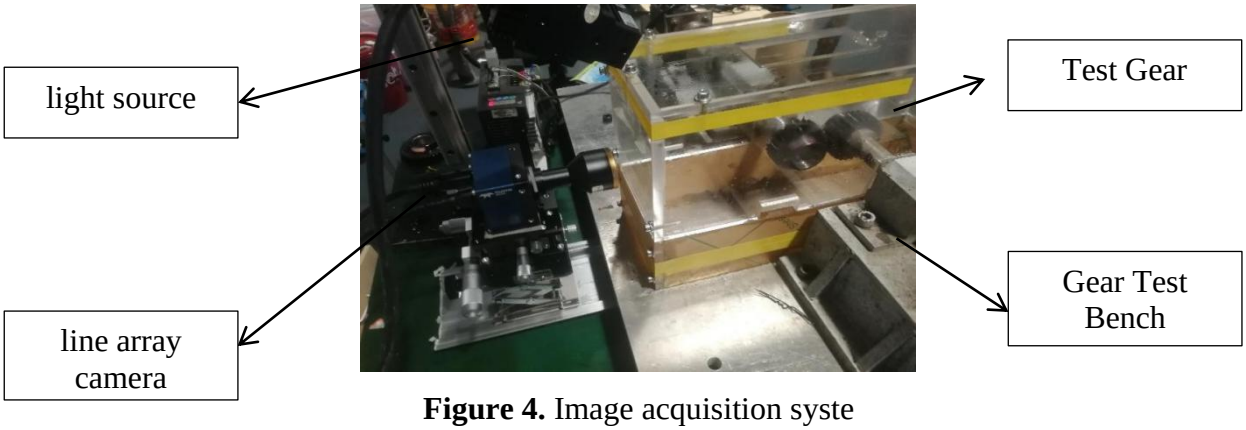

Figure 4. Image acquisition syste

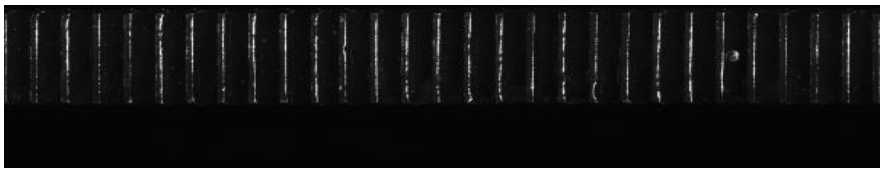

Figure 5. Original drawing of gear meshing surfaces

3. FAST CORRECTION ALGORITHM FOR GEAR IMAGES

From the images acquired by the real-time gear contact fatigue detection system, it can be seen that there are serious aberrations in the acquired images of the gear meshing surfaces, and if the aberration correction cannot be performed on the acquired images, the detection results of the pitting region of the gears will be seriously deviated.

According to the meshing theory of involute gears and the imaging principle of the scanning camera, analyzing the working process of the gear contact fatigue real-time detection system, it is found that the main reason for the distortion of the image of the gear meshing surface is that the linear velocity of the points on the gear involute is inconsistent with the linear frequency set by the camera, therefore, by calculating the pixel value of the imaging surface of the meshing surface through the gear parameter and the value of the meshing surface of the gear photographed by the camera, the image of the meshing surface of the gear can be corrected by this scaling ratio. Gear meshing surface correction algorithm is proposed in the paper of real-time detection method of gear contact fatigue pitting based on machine vision [1], which needs to be divided into points for many times in practical application, and then calculate the actual parameter imaging value of gear meshing surface by curve integration method, which has high computational complexity and large computational volume, and has limitations for the real-time of gear contact fatigue detection system.

Therefore, this paper proposes a fast correction algorithm for gear images. Based on the results of a large number of gear contact fatigue tests, it is found that most of the fatigue pitting of gears begins to appear pitting cracks near the pitch circle, and then gradually expands to the root circle [2], therefore, most of the fatigue pitting of gears occurs near the pitch circle, so that when calculating the actual value of the gear mesh surface, it is possible to divide the gear mesh surface into the top circle to the pitch circle and the pitch circle to the root circle, which will reduce the complexity of the calculations and lower the Calculation amount. In addition to using the idea of straight instead of curved, use the line segment of the tooth apex point and the indexing circle point instead of this involute curve, use the cosine theorem of the triangle to calculate the length of the line segment, and use this method instead of the curve product formula [1], so as to improve the detection speed. The gear image fast correction algorithm improves the detection speed, reduces the computational complexity, and realizes the real-time requirements of the gear contact fatigue detection system.

The gear image fast correction algorithm is constructed based on the principle of gear meshing and the principle of scanning camera imaging. The selected test gears are straight-toothed cylindrical involute gears, following the meshing principle of involute gears, the area imaged by the camera is the surface of the arc *KQ* from the tooth root circle to the tooth apex circle of the gears, i.e., from the point *K* to the point *Q* in Fig. 5, so the length of the arc *KQ* is the actual length of the gear meshing surface, and the actual pixel value of the gear meshing surface can be obtained by the conversion equation of the image original.

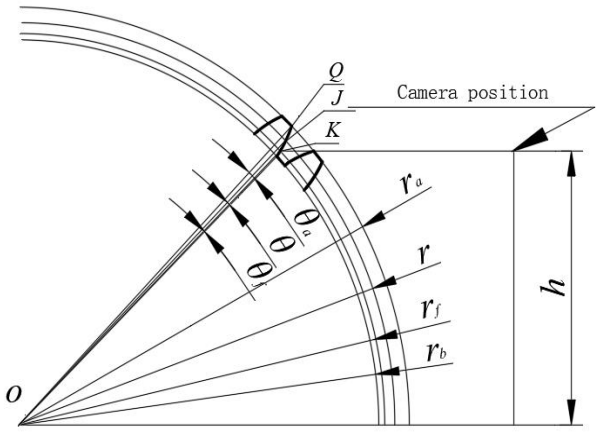

Figure 6. Photograph of gear meshing surface

3.1. Image Acquisition System Construction

From the previous analysis, it can be seen that the actual length of the gear meshing surface is the length of the arc of the circle KQ. Since the meshing surface of a pair of involute gears with the same number of teeth was used in the test and a standard mounting method was used, the radius of the pitch circle of the gear is the radius of the index circle. The arc KQ is divided into arc KJ and arc JQ by a point J on the index circle, and the line segment LKJ and line segment LJQ are used instead of arc KQ, thus avoiding the multi-segmented product formula for the arc length of the curve [1], which will reduce the complexity of the algorithm and improve the calculation speed.

First calculate the line segment LKJ, LKJ length can be derived by the cosine theorem of triangle OKJ, from Figure 6 can be seen that the length of the line segment OJ is the radius of the index circle r, the length of the line segment OK is the radius of the root circle rf, and then through the spreading angle of the index circle θ and the spreading angle θf of the root circle to get the angle JOK, the use of the triangle's cosine formula to derive the length of the line segment LKJ.

The radius of the indexing circle and the radius of the tooth root circle are calculated by the formula:

$$r = mz / 2 \tag{14}$$

$$r_f = mz / 2 - (h_a^* + c^*)m \tag{15}$$

In the formula, rf for the tooth root circle radius, mm, ha * for the top of the tooth height coefficient, ha * = 0.8; c * for the top gap coefficient, c * = 0.25, the rest of the parameters have the same meaning as before.

The indexing circle spread angle is calculated by the formula:

$$\begin{aligned} \theta &= \text{inva} = \tan a - a \\ r_b &= \frac{mz}{2}\cos a \end{aligned} \tag{16}$$

The tooth root spread angle is calculated as:

$$\begin{aligned} \theta_f &= \text{inva}_f = \tan a_f - a_f \\ r_f &= r_b / \cos a_f \end{aligned} \tag{17}$$

The spread difference between the index circle and the root circle is angle KOJ, denoted θ of, and the cosine theorem for angle θ of in triangle KOJ is:

$$L_{KJ}^2 = r^2 + r_f^2 - 2rr_f\cos(\theta_{of}) \tag{18}$$

Similarly, the length of the line segment LJQ can be deduced from the radius and spreading angle calculation formula of the tooth apex circle. The actual length of gear meshing surface LKQ can be obtained from the length of line segment LKJ and line segment LJQ, and the actual length of gear meshing surface LKQ can be converted into the actual pixel value of gear meshing surface WKQ by the like-original conversion formula, and the like-original conversion formula is:

$$W_{KQ} = \frac{\beta L_{KQ}}{l} \tag{19}$$

Where β is the camera magnification, β = 0.2; l is the pixel size, l = 7.04 um.

3.2. Derivation of Pixel Values for Imaging Gear Meshing Surfaces

According to the image acquired by the gear contact fatigue real-time detection system, the image of each tooth of the gear image consists of two parts, one is the image of the gear meshing surface, and the other is the Image of the toothed top circle of a gear. According to the gear fatigue pitting occurs in the vicinity of the pitch circle and gradually expands to the root circle [2], therefore, the scanning frequency of the camera can be set based on the pitch circle circumference, and the gear contact fatigue detection system adopts a pair of gears with the same number of teeth for the standard installation of the mesh, so the circumference of the indexing circle is the pitch circle circumference.

From the scanning camera imaging process can be known, when the gear rotates through a certain angle of the time used is recorded as t, the camera imaging pixel value in t time is equal to the product of line frequency and time t, therefore, analyze the gear mesh surface rotation process can be deduced from the gear mesh surface imaging time used.

The rotation analysis process of the gear meshing surface is shown in Fig. 7, the gear is rotated from point *Q* to point *P* for the period of time, which is denoted as t_{PQ}, and at this time the camera captures an image of the gear meshing surface, so the pixel value of the imaging of the gear meshing surface can be deduced by solving for t_{PQ}.The rotation angle corresponding to the time t_{PQ} is $\theta_{PQ,}$ and the value of the rotation angle θ_{PQ} is related to the difference θ_{af} between the tooth apex spread angle and the tooth root spread angle, as well as the difference β_{af} between β_f and β_a.

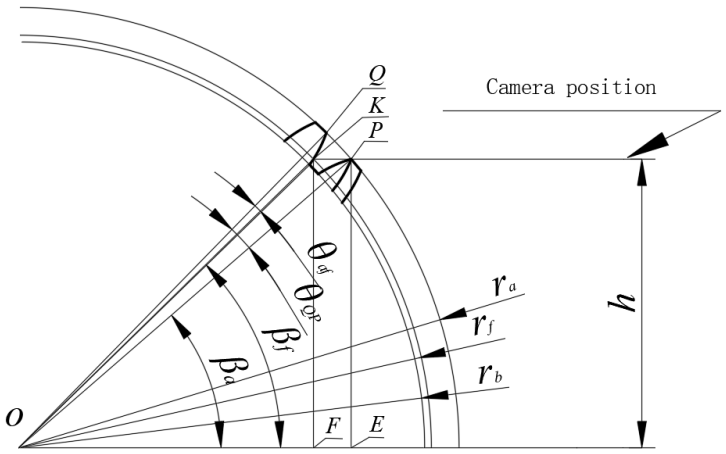

Figure 7. Rotational analysis of gear meshing surfaces

The difference in spreading angle θ_{af} between the tooth apex circle and the tooth root circle can be deduced from the involute gear spreading equation. The tooth apex circle spreading angle θ_f is obtained from the formula in section 3.1, and the tooth apex circle spreading angle θ_a is found by the

same reason.The difference between the spread angle of the tooth apex circle and the tooth root circle, θ_{af}, is deduced to be:

$$\theta_{af} = \theta_a - \theta_f \tag{20}$$

From Fig. 5, it can be seen that β_f and β_a belong to right triangle *KOF* and right triangle *KOE*, respectively, and the values of β_f and βa are calculated from the right triangle function.

$$\begin{aligned} \beta_a &= \arcsin(h / r_a) \\ \beta_f &= \arcsin(h / r_f) \\ \beta_{af} &= \beta_f - \beta_a \end{aligned} \tag{21}$$

This leads to the derivation of the rotation angle θ_{PQ} as:

$$\theta_{PQ} = \theta_{af} + \beta_{af} \tag{22}$$

The nominal speed of the gear n = 500 r/min and the time t_{PQ} taken to turn the angle θ_{PQ} is:

$$t_{QP} = \frac{60\theta_{PQ}}{2\pi n} \tag{23}$$

The imaged pixel value of the gear meshing surface, denoted as W_{PQ}:

$$W_{PQ} = t_{PQ} LF \tag{24}$$

Where: W_{PQ} is the pixel value imaged on the gear meshing surface, *pixel*; t_{PQ} is the time used by the camera to image the gear meshing surface, *s*; *LF* is the line frequency of the camera scanning, *pixel/s*.

3.3. Gear Meshing Surface Image Extraction and Distortion Correction

The acquired gear image is each tooth image, which consists of two parts: the meshing surface image of the gear and the top circle image of the tooth, and there is a periodicity between each tooth, so the periodicity can be utilized to extract the meshing surface image of the gear. From section 3.2, it is known that the pixel value of the gear meshing surface imaging is WPQ, and then based on the number of teeth Z of the gear and the camera set the image width W, the pixel area occupied by each tooth can be obtained, so as to extract the image of the meshing surface of each tooth, as shown in Fig. 8.

The actual pixel value of the gear meshing surface, WKQ, is derived from Section 3.1, and the imaged pixel value of the gear meshing surface, WPQ, is derived from Section 3.2. Therefore, in conjunction with the scanning camera characteristics, the pixel overlap causes the tooth profile image to have a stretch in the horizontal direction and no stretch in the vertical direction. Noting that the transverse and longitudinal expansion ratios of the gear meshing surfaces are Px and Py, respectively, then:

$$p_x = \frac{W_{KQ}}{W_{PQ}}, \; p_y = 1 \tag{25}$$

The corrected image of the gear meshing surface taking into account the effect of overlapping pixels is obtained by multiplying the gear meshing surface image by its corresponding image scaling (px,

py). During the test, in order to ensure that the size of the corrected image better matches the actual meshing surface, the scaling transformation of the meshing surface image was performed using the cubic interpolation method. The cubic interpolation function has the advantage of solving the trapezoidal boundary problem of nearest-neighbor interpolation, and it deals well with the blurring problem caused by linear interpolation, and keeps the details of the image very well. After the gear meshing surface fast correction algorithm processing results are shown in Figure 8.

Figure 8. Processing results of gear meshing surface fast correction algorithm

3.4. Gear Meshing Surface Image Extraction and Distortion Correction

By observing the gear meshing surface image, it can be concluded that the gear meshing surface image of the gear without pitting is at a low gray value and belongs to the background, and when pitting occurs on the gear meshing surface the gray value is larger and belongs to the foreground, i.e., it is the pitting feature that needs to be extracted. The area growth segmentation method is used to process the gear meshing surface image, and then the real gear pitting pit is screened out by similar region fusion, area feature extraction or area average gray value extraction, and finally the test gear pitting area is obtained, which is noted as Sd, and the pitting feature extraction is shown in Fig. 9. Then combined with the total area of the gear meshing surface SZ, the pitting rate of the gear can be obtained, the pitting rate of the gear is denoted by η, and the total area of the gear meshing surface is:

$$S_z = ZW_{KQ}W_B \tag{26}$$

Where: WKQ is the pixel value of the gear meshing surface of a single tooth, pixel; WB is the pixel value of the tooth width of a single tooth, pixel, and Z is the number of gear teeth.

The gear pitting rate η is:

$$\eta = (S_d / S_Z) \times 100\% \tag{27}$$

In accordance with GB/T14229-93 "gear contact fatigue strength test method" stipulated in the gear fatigue failure determination standard, when the test gear pitting area rate of 2% is considered to be failure [15]. This can determine whether the test gear fatigue failure, thus realizing the test system intelligent shutdown or continue the test.

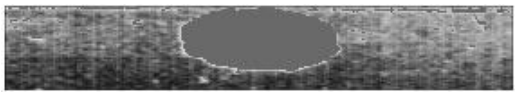

Figure 9. Gear pitting characteristics

4. RESULTS

In order to verify the feasibility of the image acquisition system and the effectiveness of the contact fatigue detection method, pitting pits of different area sizes were randomly punched on the gear face, and 10 of the 500 gear images acquired by shooting were randomly selected as testing samples. Photographs of the gear meshing surfaces taken under the SZX12 microscope at a magnification of 20 times were labeled with pitting pits, and this was taken as the true value, and the captured images are shown in Fig. 10.The original detection algorithm is the gear meshing surface correction algorithm proposed in the paper real-time detection method of gear contact fatigue pitting based on machine

vision [1], and the fast algorithm is the gear image fast correction algorithm proposed in this paper, and these two algorithms are compared with the real value respectively, and the relative error and absolute error are calculated, and the experimental results are shown in Table 4.1.

The statistics of the experimental results show that: the average relative error of the original algorithm for gear pitting area detection, i.e., the gear meshing surface correction algorithm, is 2.428%, and the average absolute error is 0.1263mm2; the average absolute error of the fast algorithm for detection, i.e., the fast gear image correction algorithm proposed in this paper, is 2.2868%, and the average absolute error is 0.11059mm2. The algorithm proposed in this paper shows a decrease of 0.1412% in absolute error and 0.0127mm2 in relative error in gear pitting area detection compared to the gear meshing surface correction algorithm [1].

Table 4.1. Gear pitting area test results

Data group	R/mm2	OD/mm2	OR/%	OA/mm2	FD/mm2	FR/%	FA/mm2
1	3.2789	3.3745	2.82	0.0925	3.3214	1.29	0.0425
2	3.8721	3.6102	3.76	0.2619	3.9751	2.66	0.1030
3	4.2176	4.0127	4.64	0.1959	4.0245	4.578	0.1931
4	5.3124	5.2315	1.52	0.0809	5.4127	1.89	0.1003
5	5.4781	5.3786	1.81	0.0995	5.3147	2.98	0.1634
6	4.5786	4.6234	0.98	0.0448	4.4978	0.97	0.0448
7	3.8621	3.8141	1.24	0.0480	3.7952	1.73	0.0669
8	5.9214	5.7813	2.37	0.1373	5.8314	1.52	0.090
9	6.5216	6.3412	2.76	0.1804	6.6757	2.36	0.1541
10	5.1356	5.2579	2.38	0.1223	5.2834	2.89	0.1478

In Table 4.1: R denotes the true value, OD denotes the original algorithm detection value, OR denotes the original algorithm relative error, OA denotes the original algorithm absolute error, FD denotes the fast algorithm detection value, FR denotes the fast algorithm relative error, and FA denotes the fast algorithm absolute error.

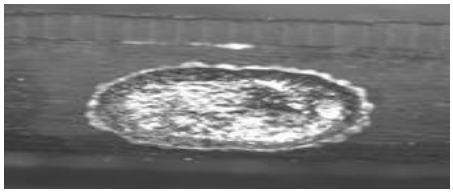

Figure 10. Microscopic image of pitting pits

5. CONCLUSIONS

The above experimental results show that the fast gear meshing surface correction algorithm proposed in this paper has a slight improvement in the accuracy of detecting the pitting pit area of gears compared with the original algorithm, and the relative and absolute errors of the fast algorithm compared with the original algorithm have been reduced, mainly due to the reduction in the amount of parameters of the fast gear meshing surface correction algorithm, which makes the algorithm more concise and reduces the model error and calculation error, and the fast algorithm's computational complexity is 1/5 of the original algorithm. In addition, the gear image fast correction algorithm adopts the straight instead of curved trigonometric function calculation method instead of the involute parametric equation curve product formula, which further improves the calculation speed, and then combines with the given gear pitting rate calculation formula, so as to detect the exact time of gear pitting failure in real time.

ACKNOWLEDGEMENTS

Author Contributions: Conceptualization, Hai Li; Data curation, Hai Li and Xiaoyang Wang; Formal analysis, Hai Li; Funding acquisition, Xiaoyang Wang and Shihui Wu; Methodology, Hai Li; Supervision, Songze Ye; Validation, ShiHui Wu and Hai Li; Visualization, Songze Ye; Writing – original draft, Hai Li; Writing –review & editing, Shihui Wu.

Funding Statement: This work was supported by the Chongqing Natural Science Foundation Upper-level Project (CSTB2023NSCQ-MSX1069); Chongqing College of Humanities and Technology School Level Project (CRKZK2024002); Chongqing College of Humanities and Technology School Level Project (CRKZK2021003); Science and Technology Project of Chongqing Municipal Education Commission (KJQN202101801); Chongqing Municipal Education Commission Scientific Research Technology Project Youth Project (KJQN202001802);

Disclosures.The authors declare no conflicts of interest.

Data availability. No data were generated or analyzed in the presented research.

REFERENCES

[1] LIU Huaiju, ZHANG Boyu, ZHU Caizhao, WEI Peitang. Progress of contact fatigue theory of gears [J]. Journal of Mechanical Engineering, 2022, 58(3):95-120.

[2] H. Li, V. Zeng, P. Kingland, P. Zhao, et al. Real-time detection method of gear contact fatigue pitting based on machine vision [J]. Formation Technology and Production Modernization, 2021, 38(04):11-21.

[3] SOLAZZI L, PETROGALLI C, LANCINI M. Vibration Based Diagnostics on Rolling Contact Fatigue Test Bench [J]. Procedia Engineering, 2011(10): 3465–3470.

[4] Xia Limin, Cai Nanping, Yang Baoxuan. Rail surface defect detection based on image differences and visual contrasts [J]. Computer Engineering and Design, 2014, 35 (06): 2052-2055.

[5] Xiong Jian, Liao Haisan, Xu Gaopeng, Yang Yan. Real-time detection method of sample contact fatigue based on machine vision [J]. Instrument Technology and Sensors, 2021 (06): 115-122.

[6] Huang Lin, Feng Keru, Yang Yan, Li Wei, Yang Changhui. The design of the machine vision detection system for rolling contact fatigue [J]. Sensors and microsystems, 2020, 39 (10): 90-92 plus 96.

[7] Fujii M, Yoshida A, Ma J B. Rolling contact fatigue of alumina ceramics sprayed on steel roller under pure rolling contact condition [J]. Tribology International, 2006, (39):856-862.

[8] Ozan Celik, Chuan-Zhi Dong, F. Necati Catbas A computer vision approach for the load time history estimation of lively individuals and crowds [J]. Computers and Structures, 2018, 200.

[9] Xie Wenqiang. Research on display defect detection based on visual perception [D]. University of Electronic Science and Technology, 2023.

[10] Hengrui Zhang. Visual defect detection of triode based on multi-classification network [D]. Harbin Institute of Technology, 2022. DOI:10.27061/d.cnki.ghgdu.2022.001672.

[11] Chen Y. Vision-based inspection technology for weld seam external dimensions and surface defects [D]. Wuhan University, 2022. DOI:10.27379/d.cnki.gwhdu.2022.000152.